Published in final edited form as:
Bioorg Med Chem Lett. 2009 January 1; 19(1): 222–225. doi:10.1016/j.bmcl.2008.10.107.

Design and synthesis of pyrazole derivatives as potent and selective inhibitors of tissue-nonspecific alkaline phosphatase (TNAP)

Shyama Sidique[†,a,b], **Robert Ardecky**[†,a,b], **Ying Su**[a,b], **Sonoko Narisawa**[b], **Brock Brown**[a,b], **José Luis Millán**[b], **Eduard Sergienko**[a,b], and **Nicholas D. P. Cosford**[*,a,b]

[a]Burnham Center for Chemical Genomics, La Jolla, CA 10901 N. Torrey Pines Road, La Jolla, California 92037

[b]Burnham Institute for Medical Research, La Jolla, CA 10901 N. Torrey Pines Road, La Jolla, California 92037

Abstract

Tissue-nonspecific alkaline phosphatase (TNAP) plays a central role in regulating extracellular matrix calcification during bone formation and growth. High throughput screening (HTS) for small molecule TNAP inhibitors led to the identification of hits in the sub-micromolar potency range. We report the design, synthesis and *in vitro* evaluation of a series of pyrazole derivatives of a screening hit which are potent TNAP inhibitors exhibiting IC_{50} values as low as 5 nM. A representative of the series was characterized in kinetic studies and determined to have a mode of inhibition not previously observed for TNAP inhibitors.

The alkaline phosphatase isozyme family in mammals is comprised of two groups, the tissue-specific alkaline phosphatases (placental, intestinal and germ cell) and tissue-nonspecific alkaline phosphatase (TNAP).[1] The major function of TNAP in bone tissue is the degradation of extracellular inorganic pyrophosphate (PP_i), a potent inhibitor of calcification, to inorganic phosphate. In this way a controlled steady state level of PP_i, is maintained, thus sustaining normal bone mineralization. Increased expression of TNAP accelerates calcification in bovine vascular smooth muscle cells (VSMCs),[2] and macrophages can induce a calcifying phenotype in human VSMCs by activating TNAP in the presence of IFNγ and $1,25(OH)_2D3$.[3] Small molecule inhibitors of TNAP therefore have the potential to probe the causative mechanisms, or treat the pathology, of diseases caused by medial calcification such as idiopathic infantile arterial calcification, end-stage renal disease and diabetes. [4-6] Until now, levamisole and theophilline were the only available inhibitors of TNAP with K_i values of 16 and 82 μM, respectively.[7] We recently reported the discovery of novel potent and selective small molecule inhibitors of TNAP using high-throughput screening (HTS).[8] Herein we report our efforts on the hit-to-lead optimization of a pyrazole TNAP inhibitor screening hit with micromolar potency to provide novel derivatives with low nanomolar *in vitro* potency and excellent selectivity for TNAP. The structures and IC_{50} data for compounds were deposited to PubChem under AID 1056 (http://pubchem.ncbi.nlm.nih.gov/assay/assay.cgi?aid=1056).

*Corresponding author.
†These authors contributed equally to this work.

High throughput screening (HTS) of 66,000 compounds using a luminescence-based assay[9, 10] (see PubChem link to AID 1056 for details) developed in the Burnham Center for Chemical Genomics (BCCG) led to the identification of the pyrazole derivative CID-646303 (**1** in Figure 1). Preliminary hit follow up was accomplished by performing similarity searches on databases of commercially available analogues. In this initial phase, 50 commercial analogues were identified, purchased and tested for their ability to inhibit TNAP. This allowed us to define some important features of the structure-activity relationships (SAR). For example, the potency in this series was improved from IC_{50} = 0.98 μM for the lead pyrazole **1** to IC_{50} = 0.50 μM for the 2,4-dichlorophenyl ester derivative **2** (Figure 1). Furthermore, conversion of the tricyclic derivative **3,** with an IC_{50} value of 1.33 μM, to the pyrrolidine amide analogue **4** led to a 3-fold improvement in potency (IC_{50} = 0.50 μM). Encouraged by these results we designed and synthesized two focused libraries of substituted pyrazole amide analogues. In order to optimize the potency of the hit structure the pyrazole acid scaffold **8** was selected as the key synthon for the preparation of amide analogues (Scheme 1).

The synthetic chemistry used for the preparation of the pyrazole acid scaffolds is shown in Scheme 1. Reaction of acetophenone derivatives **5** with sodium methoxide and dimethyl oxalate yielded the 1,3-diketone derivatives **6** in excellent yields (75–90%). Compound **6** was then reacted with hydrazine to give the corresponding pyrazole ester **7**. Saponification of the methyl ester provided access to the pyrazole acids **8**.

The synthetic chemistry used for hit optimization is shown in Scheme 2. The pyrazole acid **8** was treated with HOBT, EDC and DIEA to produce the amides **9**[11] or the desired hydrazide derivative **10**.

In light of the preliminary data generated from the HTS hits and commercial analogues our goal was to determine the key components of the SAR required for potency. For the focused library synthesis we selected a 2,4-dichloro and 2,4-dichloro-5-fluoro substitution pattern for the phenyl ring based on the initial SAR data. In the first library, twenty six compounds were synthesized and tested in the *in vitro* assay. This led to the identification of four analogues with potency values of 100 nM or better (Table 1). The incorporation of a hydroxyl group on the amide generally increased potency (**9a** and **9j**). In all cases the 2,4-dichloro analogues were more potent than the corresponding 2,4-dichloro-5-fluoro analogues (Table 1). A second generation set of pyrazoles consisting of a library of twenty eight compounds were synthesized next (Table 2). In this series we found that branching of the amides generally decreased potency in the *in vitro* assay, especially when the chain length was greater than three carbon atoms. We also observed that amides with chain lengths of three carbons or less were the most active (Tables 1 and 2).

In the second series, when the hydroxyethyl chain was increased by one or two additional carbon atoms (**9m**, **9n**), or a second hydroxyethyl side chain was added (**9p**), these changes did not affect the potency of the initial hit **9a** (Tables 1 and 2). The most potent compound in this series was the 2,3,4-trichlorophenyl analogue **9v** (Table 3). This compound showed exceptional activity with an *in vitro* IC_{50} of 5 nM (Table 3). Furthermore, compound **9v** was inactive (IC_{50} > 10 μM) against both the related placental alkaline phosphatase (PLAP) isozyme and the house keeping enzyme glyceraldehyde-3-phosphate dehydrogenase (GAPDH), indicating a selectivity for TNAP of at least 2000-fold.

We next performed a series of experiments to elucidate the mechanism of action (MOA) of the novel TNAP inhibitors. The catalytic mechanism by which TNAP degrades PP_i consists of rapid phosphorylation of the active site in the presence of the phosphor-donor substrate and a rate-limiting dephosphorylation by the phospho-acceptor substrate, either water or amino-containing alcohols (Figure 2). All the TNAP inhibitors known to date are uncompetitive with

respect to phospho-donors[7,8] and are likely to be non- or uncompetitive with diethanolamine (DEA).

The latter conclusion is based on the fact that the majority of the alkaline phosphatase assays are performed in the presence of saturating concentrations of DEA or other phosphor-acceptors.[9]

To characterize the mode of action (MOA) of the novel TNAP inhibitor series we selected compound **9v** for additional studies. By performing detailed kinetic studies,[13] we demonstrated that **9v** is competitive with respect to both substrates, the water-soluble 1,2-dioxetane reagent disodium 2-chloro-5-(5′-chloro-4-methoxyspiro[1,2-dioxetane-3,2′-tricyclo[3.3.1.13,7] decan]-4-yl)-phenol-1-(dihydrogen phosphate) (CDP-star) and DEA (Figure 3). This is the first time that a competitive MOA has been established for an inhibitor of TNAP.

To gain some structural insight into how the inhibitors interact with TNAP protein, we performed *in silico* docking studies to investigate the potential binding mode of **9a** in the active site of TNAP using the Schrodinger Glide program.[14]

Since the TNAP 3-dimensional crystal structure is not available, a homology model, built using the placental alkaline phosphatase (PLAP) crystal structure (PDB code: 1EW2) as the template, was used for docking[15]. The sequence identity of TNAP and PLAP is 56% according to the sequence alignment algorithm blastp provided by NCBI BLAST (http://blast.ncbi.nlm.nih.gov/), while the homology is 74%. The binding mode suggested by Glide is shown in Figure 4. In this model, the carbonyl of the amide chain coordinates to the Zn^{2+} ion and the 2,4-dichloro phenyl ring of compound **9a** contributes to the binding through a stacking interaction with the side chain of Tyr371.

In agreement with the importance of the stacking interaction, replacement of the phenyl group by an acyl group results in complete loss of activity (data not shown). Compound **9a** was docked into the catalytic site either with serine 93 phosphorylated or with free serine 93. Interestingly, the binding modes are the same, suggesting that compound **9a** functions as a competitive inhibitor. This predicted inhibition mechanism is consistent with the kinetic/mechanistic studies.

In summary, we have described the design, synthesis and chemical optimization of a series of pyrazole amide derivatives that are potent inhibitors of TNAP. The hit-to-lead optimization of the screening hit **1** led to compound **9v**, which is approximately 200 times more potent against TNAP, and shows a high degree of selectivity against the related PLAP isozyme. Mechanistic studies demonstrated a novel MOA for **9v**, and these data were supported by *in silico* docking studies. Compound **9v** should prove to be an extremely useful small molecule tool to facilitate investigations into the biochemistry and pharmacology of TNAP.

Acknowledgments

This work was supported by NIH grants U54HG003916 and DE12889.

References

1. Millán, JL. Mammalian alkaline phosphatases. From biology to applications in medicine and biotechnology. Wiley-VCH Verlag GmbH & Co; Weinheim, Germany: 2006. p. 1-322.
2. Shioi A, Nishizawa Y, Jono S, Koyama H, Hosoi M, Morii H. Arterioscler Thromb Vasc Biol 1995;15:2003. [PubMed: 7583582]
3. Shioi A, Katagi M, Okuno Y, Mori K, Jono S, Koyama H, Nishizawa Y. Circ Res 2002;91:9. [PubMed: 12114316]

4. Lomashvili KA, Garg P, Narisawa S, Millan JL, O'Neill WC. Kidney Int 2008;73:1024. [PubMed: 18288101]
5. Addison WN, Azari F, Sorensen ES, Kaartinen MT, McKee MD. J Biol Chem 2007;282:15872. [PubMed: 17383965]
6. Kaunitz JD, Yamaguchi DT. J Cell Biochem 2008;105:655. [PubMed: 18773425]
7. Kozlenkov A, Hoylaerts MF, Ny T, Le Du MH, Millán JL. J Bone Miner Res 2004;19:1862. [PubMed: 15476587]
8. Narisawa S, Harmey D, Yadav MC, O'Neill WC, Hoylaerts MF, Millán JL. J Bone Miner Res 2007;22 (11):1700. [PubMed: 17638573]
9. Sergienko EA, Millán JL. unpublished results
10. TNAP activity was measured on an EnVision plate reader in the presence of 100 mM diethanolamine-HCl, pH 9.8, 1 mM $MgCl_2$, 20 μM $ZnCl_2$, and 50 μM CDP-star.
11. Representative synthesis of **9v**: A mixture of 2,3,4-trichloroacetophenone (4.46 g, 0.02 mol) and dimethyl oxalate (2.36 g, 0.02 mol) was dissolved in Et_2O (100 mL) and stirred at room temperature. To this solution was added a freshly prepared solution of NaOMe, prepared from sodium metal (0.55 g, 0.0024 mol) dissolved in MeOH (10 mL). A yellow precipitate immediately formed and the reaction was stirred for 1 h at room temperature. The precipitate was filtered and dissolved in water (200 mL) and the solution was adjusted to pH 3 with HOAc. The resulting precipitate was filtered and dried to give 5.20 g (84%) of methyl 2,4-dioxo-4-(2,3,4-trichlorophenyl)butanoate (**6**). A mixture **6** (5.20 g, 0.018 mol) and HOAc (100 mL) was stirred at room temperature. To this solution was added hydrazine (7.5 mL, 0.24 mol) and the reaction mixture was stirred overnight. The precipitate was filtered, washed with hexane and dried to give 5.19 g (95%) of methyl 3-(2,3,4-trichlorophenyl)-1H-pyrazole-5-carboxylate (7). A mixture of 7 (5.19 g, 0.017 mol), MeOH (100 mL), THF (100 mL) and LiOH solution (2M, 10 mL) was heated at reflux overnight. The reaction was cooled and the solvents removed under reduced pressure. The residue was dissolved in water (100 mL) and EtOAc (100 mL) and the pH of the solution was adjusted to neutral with 1 M HCl. The organic layer was separated, dried and the solvents were removed under reduced pressure to give 5.01 g (96%) of 3-(2,3,4-trichlorophenyl)-1H-pyrazole-5-carboxylic acid (**8**). A mixture of **8** (0.29 g, 0.001 mol), EDC (0.19 g, 0.001 mol), HOBt (0.14, 0.001 mol) and DMF (10 mL), was stirred for 1 h. To this solution was added ethanolamine (1 mL, 0.017 mol). The reaction was stirred overnight and the solvents were removed under reduced pressure. The residue was dissolved in EtOAc (25 mL) and water (25 mL). The organic layer was separated, and washed with HCl (1 M) followed by sat. sodium bicarbonate solution and the organic layer was dried over magnesium sulfate and evaporated. The residue was purified using automated medium pressure silica gel chromatography (ISCO) eluting with DCM:EtOAc 100:0 to 70:30 gradient to yield 0.27 g (80%) of **9v**. ^1H NMR (300 MHz, DMSO-d_6,TMS) δ 8.48 (s, 1H), 7.71 (s, 2H), 7.34 (s, 1H), 4.82 (s, 1H), 3.54-3.35 (m, 4H); ^{13}C NMR (75 MHz, DMSO-d_6,TMS) δ 160.3, 145.1, 142.0, 133.2, 132.4, 131.9, 131.7, 130.0, 129.7, 106.9, 60.4, 42.2. HRMS calcd. for $C_{12}H_{10}Cl_3N_3O_2$: 333.9911; found: 333.9919.
12. Holtz KM, Stec B, Kantrowitz ER. J Biol Chem 1999;274:8351. [PubMed: 10085061]
13. TNAP MOA studies: the activity of TNAP was measured in the presence of varied concentrations of substrate at different concentrations of test compound. Parallel studies were performed for DEA and CDP-star substrates. The concentration of the second substrate was maintained constant (see Figure 2 legend for details).
14. Friesner RA, Banks JL, Murphy RB, Halgren TA, Klicic JJ, Mainz DT, Repasky MP, Knoll EH, Shelley M, Perry JK, Shaw DE, Francis P, Shenkin PS. J Med Chem 2004;47:1739. [PubMed: 15027865]
15. Le Du MH, Millán JL. J Biol Chem 2002;277:49808. [PubMed: 12372831]

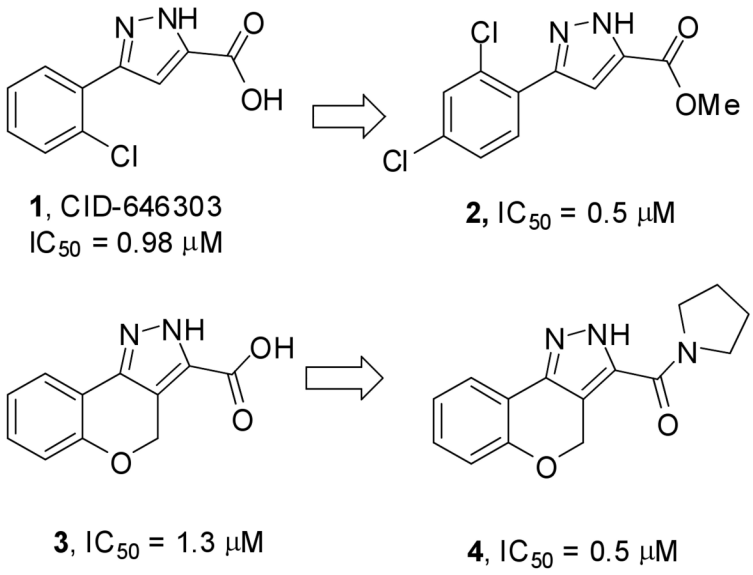

Figure 1.
Initial hit from screening and commercial analogues.

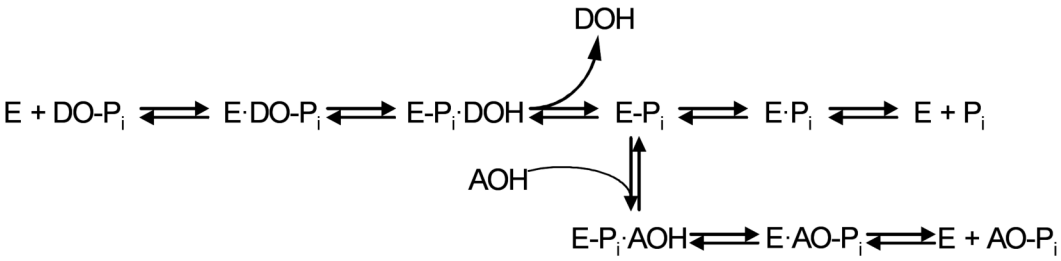

Figure 2.

The catalytic mechanism of the alkaline phosphatase reaction.[12] The initial alkaline phosphatase (E) catalyzed reaction consists of a substrate (DO-Pi) binding step, phosphate-moiety transfer to Ser-93 (in the TNAP sequence of its active site) and product alcohol (DOH) release. In the second step of the reaction, phosphate is released through hydrolysis of the covalent intermediate (E-Pi) and the non-covalent complex (E·Pi) of the inorganic phosphate in the active site. In the presence of nitrogen-containing alcohol molecules (AOH), such as the buffer diethanolamine (DEA), phosphate is also released via a transphosphorylation reaction.

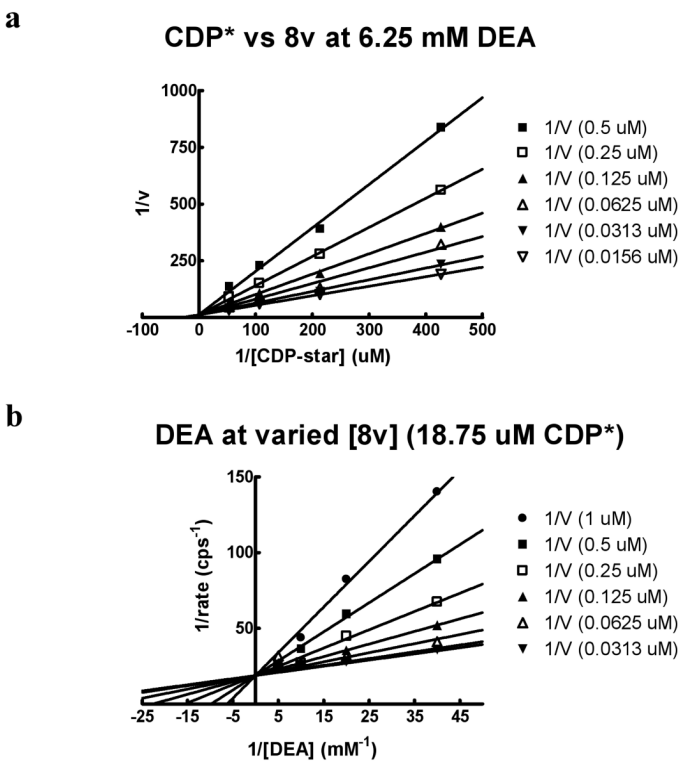

Figure 3.

Mechanism of action studies for compound **9v**: Lineweaver-Burke plots. TNAP kinetic data were obtained in the presence of (a) 6.25 mM DEA or (b) 18.8 μM CDP-star. The concentration of the second substrate was varied in the presence of different concentrations of 9**v.** Closed circle– 1000 nM, closed square – 500 nM, open square – 250 nM, closed triangle - 125 nM, open triangle – 62.5 nM, closed upside-down triangle – 31 nM, open upside-down triangle – 15.6 nM.

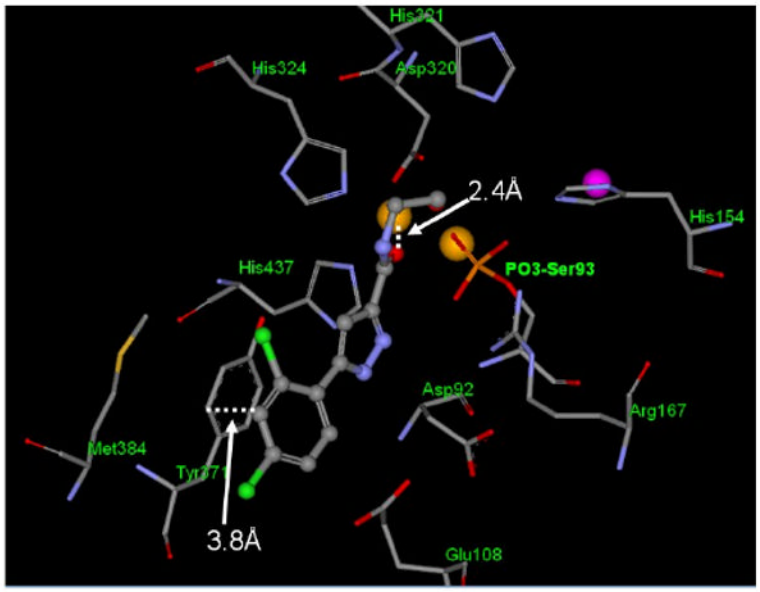

Figure 4.

Proposed binding mode of **9a** in the catalytic site of the enzyme. Compound **9a** is displayed in ball and stick mode and the protein residues within 4Å of the ligand are displayed in stick mode. Dashed lines highlight the potential key interactions between protein and **9a**. The zinc ions are shown in gold, magnesium ion in magenta.

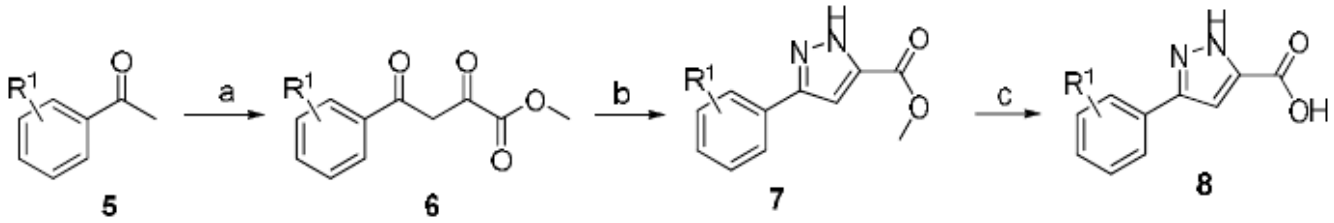

Scheme 1.

Reagents and conditions: (a) (i) NaOMe, Et_2O, dimethyl oxalate, 25 °C, 4 -12h, (ii) AcOH (75-90%); (b) N_2H_2, AcOH, 100 °C, 12 h (50-85%) (c) LiOH, THF, MeOH, reflux (90-95%).

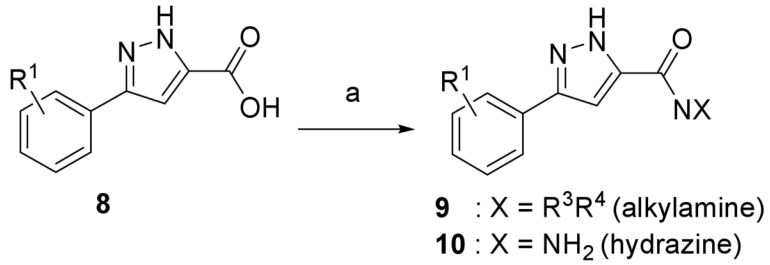

Scheme 2.
Reagents and conditions: (a) EDC, HOBT, DMF, DIEA, NH_2X (85-95%).

Table 1

Summary of *in vitro* data from first focused library.

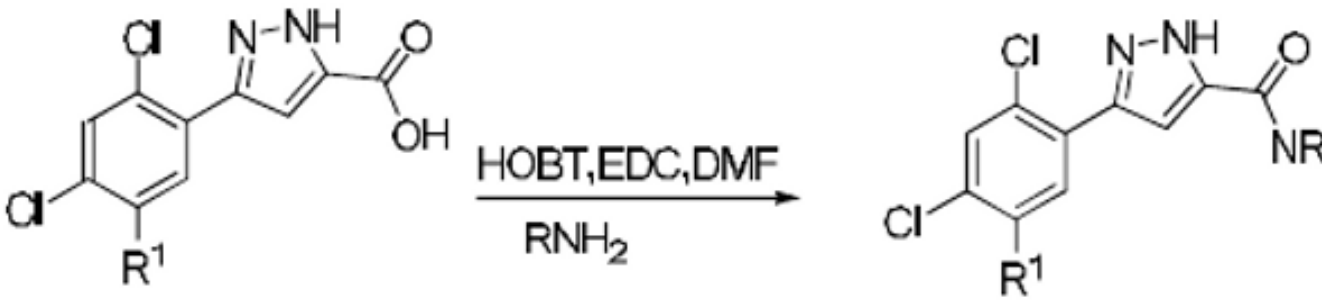

Compound	R^1	RNH_2
9a	H	$NH_2CH_2CH_2OH$
9b	H	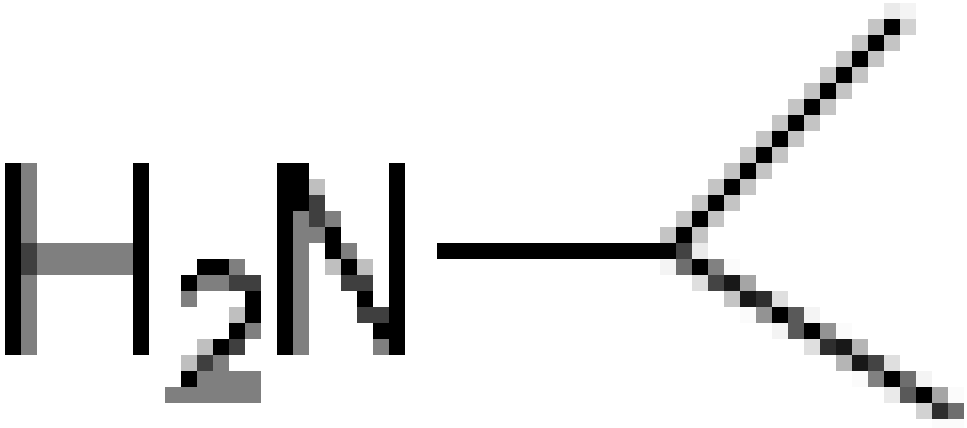
9c	H	

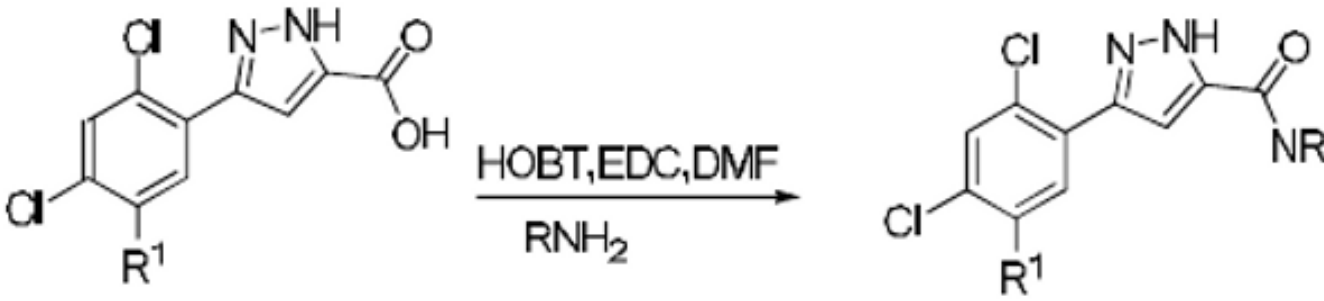

Compound	R^1	RNH_2
9d	H	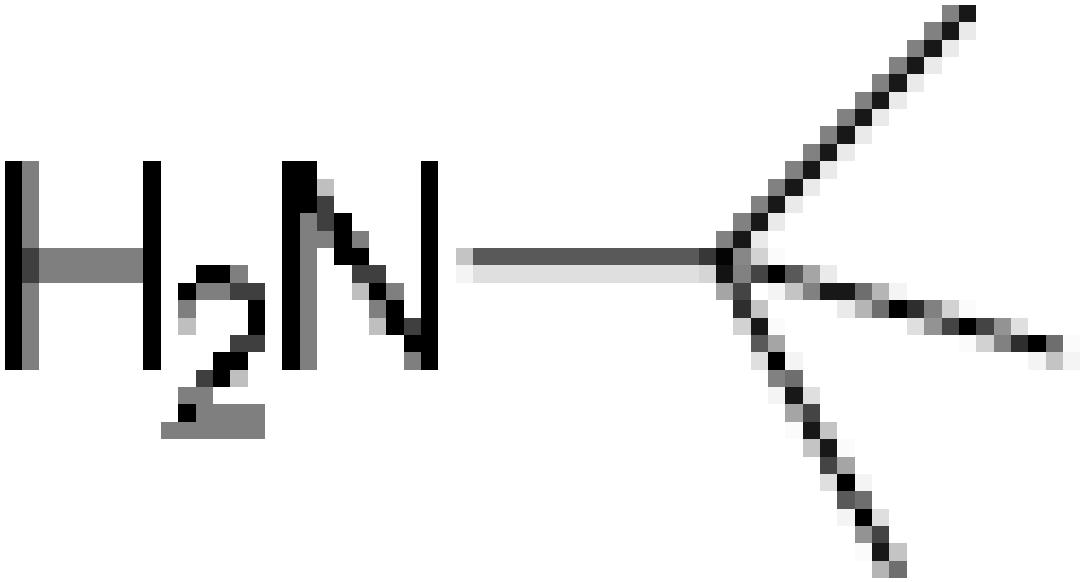

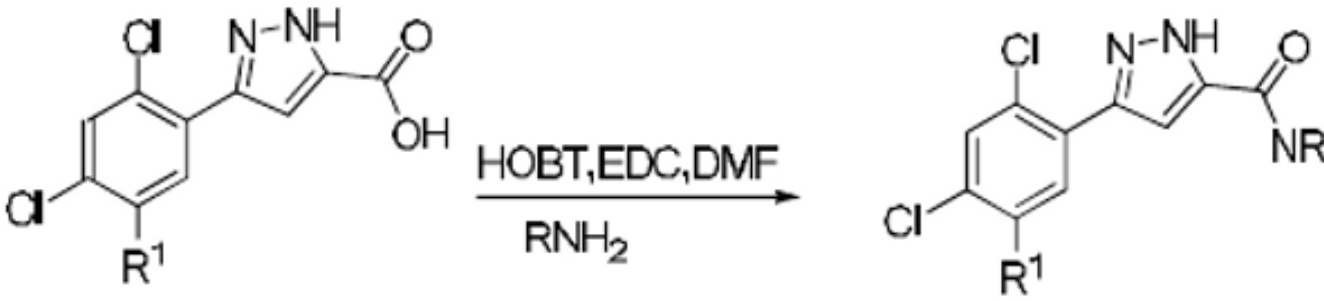

Compound	R^1	RNH_2
9e	H	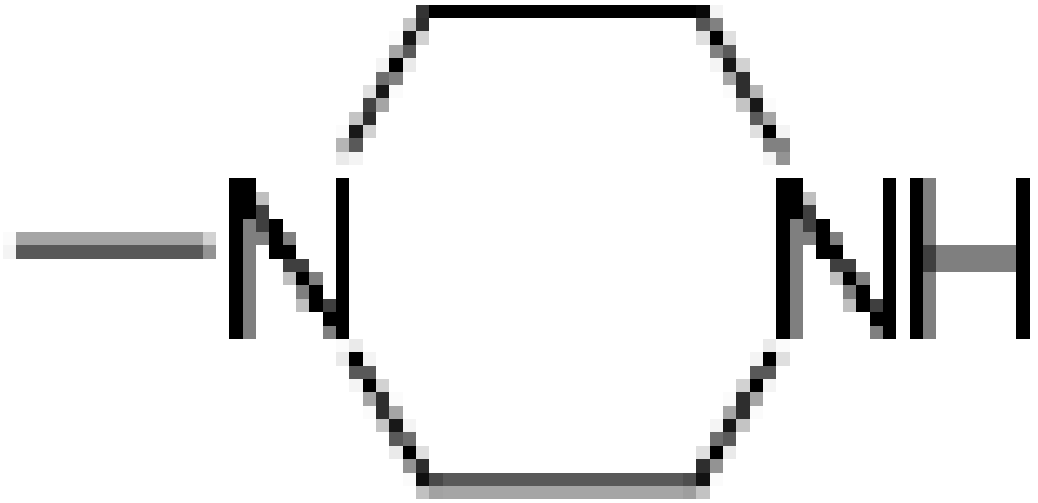
9f	H	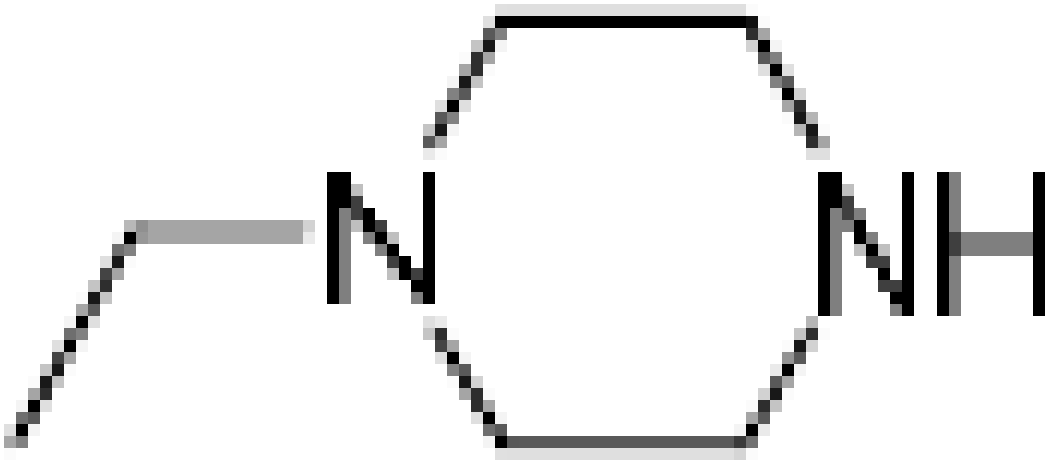
9g	H	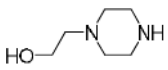

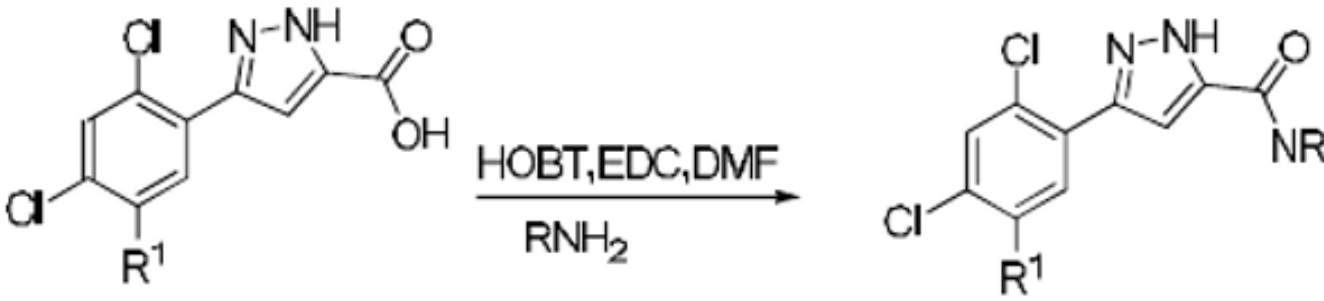

Compound	R^1	RNH_2
9h	H	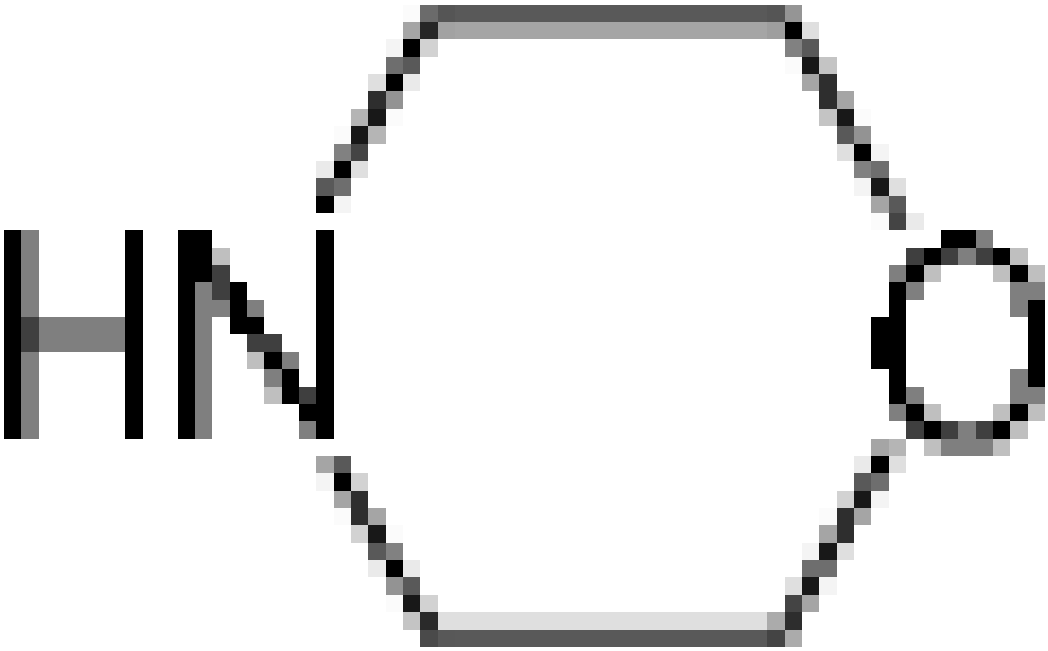

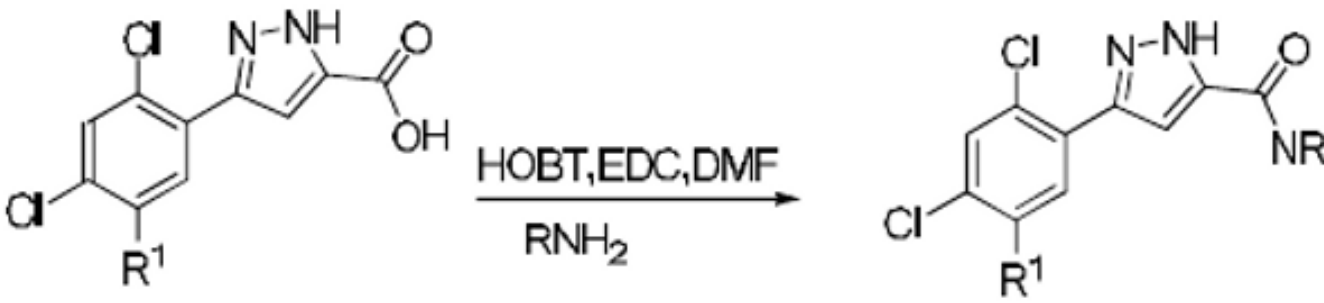

Compound	R^1	RNH_2
9i	H	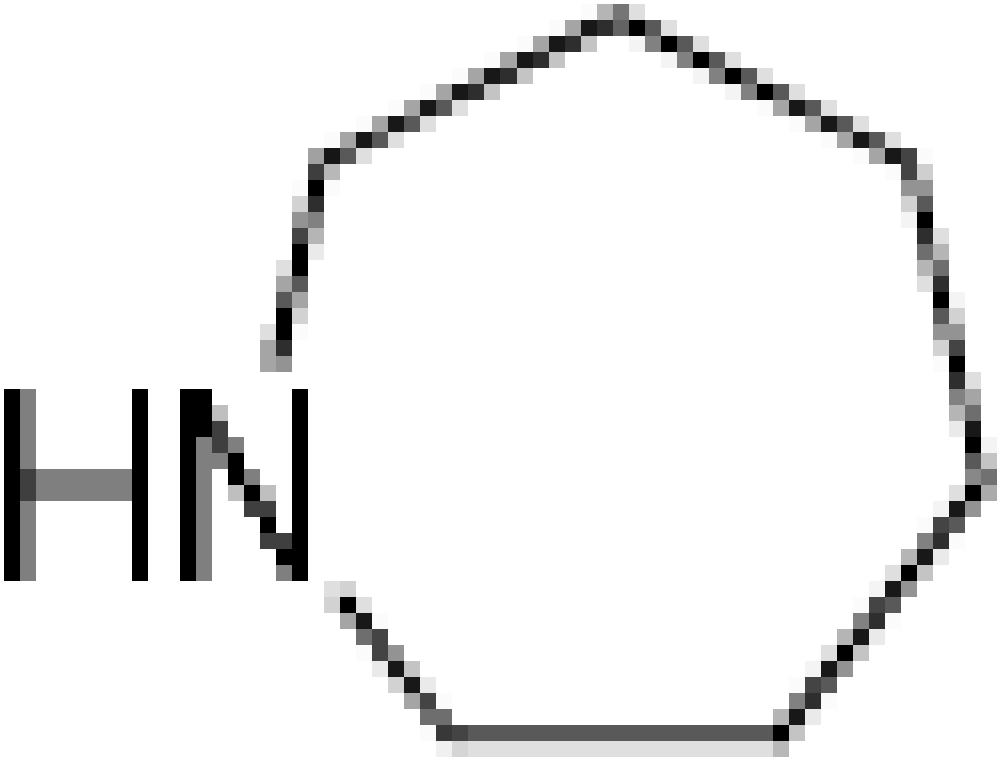
9j	F	$NH_2CH_2CH_2OH$
9k	F	
9l	F	
10	H	NH_2NH_2

Table 2

Summary of *in vitro* data from second focused library.

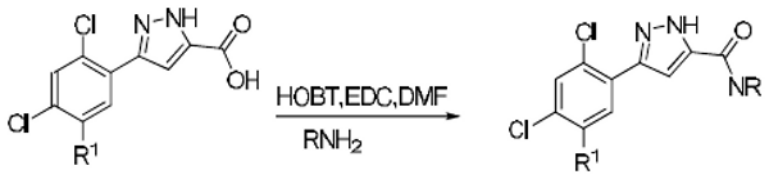

Compound	R^1	RNH_2
9m	H	$NH_2CH_2CH_2CH_2OH$
9n	H	$NH_2CH_2CH_2CH_2CH_2OH$
9o	H	$NH_2CH_2CH_2OMe$
9p	H	$NH_2(CH_2CH_2OH)_2$
9q	H	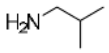
9r	H	
9s	H	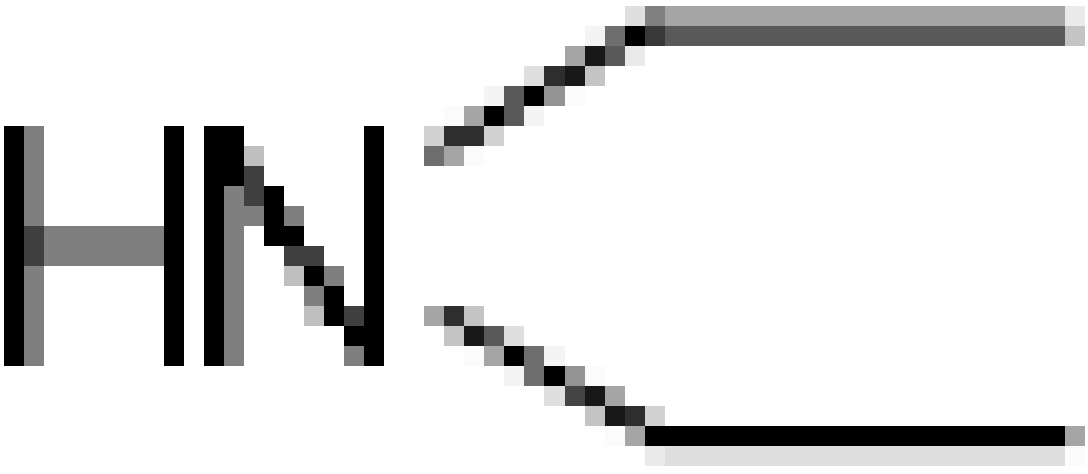
9t	F	$NH_2CH_2CH_2CH_2OH$

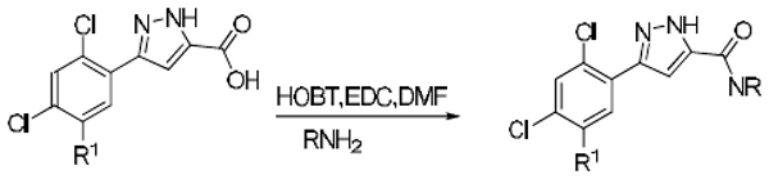

Compound	R^1	RNH_2
9u	F	$NH(CH_2CH_2OH)_2$

Table 3

Summary of *in vitro* data for trichloro- and trifluorophenyl derivatives.

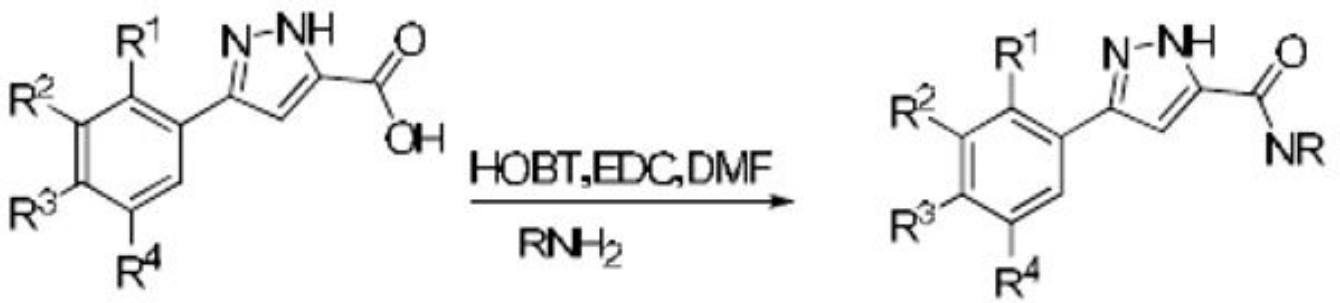

Compound	R^1	R^2	R^3	R^4	RNH_2	IC_{50} (μM)
9v	**CI**	**CI**	**CI**	**H**	**$NH_2CH_2CH_2OH$**	**0.005**
9w	F	H	F	F	$NH_2CH_2CH_2OH$	0.134
9x	F	H	F	H	$NH_2CH_2CH_2OH$	0.035